Journal of Materials Chemistry B

Accepted Manuscript

ROYAL SOCIETY OF CHEMISTRY

www.rsc.org/materialsB

PEGylated carbon nanoparticles for efficient *in vitro* photothermal cancer therapy

Xiaolong Tu,[a, b] Yufei Ma,[a] Yuhua Cao,[a,b] Jie Huang,[a] Mengxin Zhang,[a,b] and Zhijun Zhang*[a]

[a] *Suzhou Key Laboratory of Nanobiomedicine, Division of Nanobiomedicine, Suzhou Institute of Nano-Tech and Nano-Bionics, Chinese Academy of Sciences, Suzhou 215123, China*

[b] *University of Chinese Academy of Sciences, 19 Yuquan Road, Beijing, 100049, China.*

* Corresponding author. E-mail: zjzhang2007@sinano.ac.cn, Tel: 86-512-62872556, Fax: 86-512-62603079.

† Electronic supplementary information (ESI) available: XPS analysis; Raman spectra; FT-IR spectra of PCNPs and PCNPs-FITC; Thermogravimetric analysis of CNPs and PCNPs; Photographs of PCNPs in aqueous and polar organic solvents; Photothermal effect of gold nanorods and graphene oxide; MTT and LDH release assays of CNPs; UV-Vis and PL spectra of PCNPs-FITC and FITC in aqueous solution; TEM and AFM data of PCNPs and PCNPs-FITC.

Abstract

Photothermal therapy (PTT) is an emerging technique for effective cancer elimination in animal experiments. The key to the success of the PTT is to develop efficient and safe photosensitive agents. Activated carbon (AC), a widespread material safely used in routine and emergent medical services, is emerging as a nascent PTT agent. Here we report for the first time synthesis and *in vitro* PTT application of carbon nanoparticles (CNPs, less than 10 nm) derived from AC. In our strategy, CNPs are obtained via chemical oxidation and transferred to PEGylated CNPs (PCNPs) to reduce nonspecific adsorption and to improve biocompatibility. Fluorescein isothiocyanate is conjugated to PCNPs to examine time-dependent uptake by human breast cancer cells (MCF-7). Photothermal effect experiment demonstrates that PCNPs possess much stronger photothermal conversion ability than carbon dots (CDs). In the dark, PCNPs pose negligible threats to cell viability and membrane integrity, while upon near infrared (NIR) irradiation PCNPs can effectively kill cancer cells. The current work demonstrates that PCNPs can be used as an efficient and safe PTT agent.

1 Introduction

Hyperthermia has drawn wide attention due to its outstanding merits in the conquest of cancer.[1-3] Photothermal therapy (PTT), involving tissue-penetrating near infrared (NIR) irradiation (700-1000 nm),[4] employs photosensitive agents to generate hyperthermia to melt cancers. Compared with traditional cancer treatments,[5] PTT can be applied extracorporeally and selectively to destroy tumors while other tissues are left unaffected, revealing PTT a noninvasive, highly selective therapy. The last decades have witnessed the surge of various optical absorbing materials as PTT agents.[6-21] Successful cancer ablation using these PTT agents propels researchers to further study their potential clinical availability which, however, is still unknown. Activated carbon (AC) has been extensively used as a strong adsorbent in medical applications owing to its chemical stability, high adsorption ability and nontoxicity.[22-27] AC was also considered as an effective tracer for clinical sentinel lymph node mapping because of its black color.[28] Recent efforts proved the optical absorbance due to the black color provided AC with great potential in PTT,[29] similar to its allotropes (e.g., carbon nanotubes, graphene oxide).[12, 13] AC may be an ideal agent for PTT for its widespread and safe administration in patients.

Ideal PTT agents should not only effectively convert the absorbed NIR light into heat, but possess excellent physiological stability and biocompatibility. Due to the large size and lack of hydrophilic groups, AC is water-insoluble and largely increases the risk of thrombosis via intravenous injection. Fortunately, carbon dots (CDs), recently have drawn considerable attention as versatile nanomaterials.[30-32] These CDs possess excellent biocompatibility. However, most CDs reported exhibit photoluminescence which might weaken their photothermal effect.[33]

Prompted and inspired by excellent performance of AC in clinical applications and the dilemma in preparation of ideal PTT agents, in this work, we synthesize water-soluble carbon nanoparticles (CNPs) from AC and coat polyethylene glycol (PEG) on them to lessen nonspecific adsorption and improve biocompatibility.[34, 35] Photoluminescence and photothermal effect experiments reveal that PEGylated CNPs (PCNPs) possess stronger optical-absorbing ability than CDs and can effectively

transfer NIR light into heat. Cellular uptake experiment reveals an efficient and time-dependent cellular internalization behavior of PCNPs. We find that PCNPs exhibit good biocompatibility to MCF-7 cells in the dark, but cause notable cell death under NIR irradiation due to heat-induced apoptosis. Scheme 1 outlines the preparation of PCNPs and in vitro photothermal therapy. Our research presents an effective and simple way to prepare carbon-based, efficient heat-producing PTT agent.

2 Experiments

2.1 Materials and characterization

Amine-terminated six-armed PEG (10 kDa) was purchased from SunBio. 1-ethyl-3-(3-dimethylaminopropyl)-carbodiimide (EDC) and fluorescein isothiocyanate (FITC) were purchased from Sagon Biotech. 3-(4, 5-Dimethylthiazol-2-yl)-2, 5-diphenyltetrazolium bromide (MTT), trypan blue, penicillin and streptomycin were purchased from Sigma. LDH release, cell cycle arrest and apoptosis assay kits were purchased from Beyotime Institute of Biotechnology. Activated carbon and other reagents were from Sinopharm Chemical Reagent Company and used as received without further purification.

Transmission electron microscope (TEM) images were obtained from an FEI Tecnai G2 F20 S-Twin transmission electron microscope, and atomic force microscope (AFM) images were conducted on a Vecco Dimension 3100 atomic force microscope. UV-Vis spectra were collected with a Shimadzu UV-2550 spectrophotometer, and fluorescence spectra were collected with a Hitachi F4600 fluorescence spectrophotometer. Fourier transform infrared (FT-IR) spectra were conducted using a Thermo Nicolet 6700 FT-IR spectrometer with the KBr pellet technique. Dynamic light scattering and zeta potential assays were taken from Malvern Zetasizer ZS90.

2.2 Preparation of CNPs, PCNPs, PCNPs-FITC and CDs

CNPs were prepared via a modified chemical oxidation method.[32] Briefly, 0.3g of activated carbon was added in a 100 mL three-necked flask containing 15 mL of concentrated H_2SO_4 and 5 mL of fuming HNO_3. The suspension was sonicated for 10 min before it was heated at 120 ^oC for 5 min under vigorous stirring. Then the mixture was cooled down immediately, diluted with 100 mL of deionized (DI) H_2O and neutralized to pH 1-2 with $NaHCO_3$. The mixture was centrifuged (12000 rpm, 30 min) to collect CNPs. Eventually the obtained CNPs were washed thoroughly with DI water and further purified via spin dialysis (100 kDa cutoff, 4000 rpm).

Conjugation of PEG molecules to CNPs to form PCNPs were achieved by EDC chemistry. 25 mg of EDC was added in 500 mL of 50 μg/mL CNPs solution under ultrasonic condition to activate the carboxyl groups of CNPs. After 30 min activation, 20 mg of PEG was added in the activated CNPs solution under vigorous stirring. 75 mg of extra EDC was added in three equal shares every four hours and then the solution was further stirred for 24 h. Finally the obtained PCNPs were collected via spin dialysis (100 kDa cutoff, 4000 rpm).

PCNPs-FITC were synthesized by chemical coupling of isothiocyanate groups of FITC and amine groups of PCNPs. In brief, 5 mg of PCNPs were dissolved in 50 mL carbonate buffer (pH = 9.8) to deprotonate the amine groups. 0.2 mg FITC was added in PCNPs solution via stirring. After overnight reaction, PCNPs-FITC were purified by spin dialysis (100 kDa cutoff, 4000 rpm).

CDs were synthesized by chemical oxidation refluxing.[36] 0.1 g of activated carbon was added in a 100 mL three-necked flask containing 50 mL 5 M HNO_3. The suspension was refluxing at 80 ^oC for 24 h, cooled down to room temperature and neutralized to 7-8 with $NaHCO_3$. The resulted solution was dialyzed in a dialysis bag (3 kDa cutoff) for at least 24 h. Then the obtained CDs was concentrated on a rotary evaporator and filtered with a 0.22 μm filter.

2.3 Photothermal effect of PCNPs and CDs

To investigate the photothermal effect of PCNPs and CDs, 0.2 mL aqueous solutions of different concentrations (6.25, 12.5, 25 and 50 μg/mL) was irradiated under a NIR

laser (808 nm, 3 W) for 5 min respectively. A digital thermometer was used to measure the temperature during irradiation.

2.4 Cell culture

MCF-7 cells were cultured in regular Roswell Park Memorial Institute media (RPMI) 1640 medium (Corning) containing 10% fetal bovine serum (FBS, Hyclone), penicillin (100 U/mL) and streptomycin (100 U/mL) under 37 ^{o}C and 5% CO_2 in a humidified atmosphere incubator.

2.5 MTT assay

1×10^4 MCF-7 cells were seeded into each well of a 96-well plate. After 24 h incubation, the medium was replaced with 200 μL of fresh medium containing PBS buffer (control) or PCNPs of different concentrations (3.9, 7.8, 15.5, 31, 62.5, 125 and 250 μg/mL). After 24 h incubation, 20 μL of MTT solution (5 mg/mL in PBS) was added to each well. After further incubation for 4 h, 150 μL of dimethyl sulfoxide (DMSO) was added to each well to replace the culture medium and dissolve the insoluble formazan crystals. The absorbance of each well was measured using a PerkinElmer Victor 4 microplate reader at 490 nm.

2.6 LDH release

1×10^4 MCF-7 cells were seeded into each well of a 96-well plate. After 24 h incubation, the medium was replaced with 200 μL of fresh medium free of FBS containing PBS buffer (control) or PCNPs of different concentrations (2, 10, 50 and 250 μg/mL). After 24 h further incubation, LDH release assay was conducted and the absorbance of each supernatant was measured using a PerkinElmer Victor 4 microplate reader at 490 nm.

2.7 Cellular uptake of PCNPs

2×10^5 MCF-7 cells were seeded into 35-mm culture dishes and incubated with PBS buffer (control) and PCNPs-FITC (50 μg/mL) after 24 h seeding. After 6 and 24 h incubation, the medium was removed and the cells were washed 3 times using PBS. Then cells were fixed with 4% paraformaldehyde for 20 min. Fluorescence images were collected by Nikon A1 confocal laser scanning microscope under 488-nm excitation.

2.8 Photothermal treatment of MCF-7 cells with PCNPs

1×10^4 MCF-7 cells were seeded into each well of a 96-well plate. After 24 h incubation, the medium was replaced with 200 μL of fresh medium containing PBS buffer (control) or PCNPs of different concentrations (6.25, 12.5, 25, 50 and 100 μg/mL). After 24 h incubation, the cells were then irradiated for 5 min with an NIR laser (808 nm, 3 W). Initial temperature of each well was maintained at 37 ^{o}C with an electrical hotplate. After irradiation, the cell viability was evaluated using MTT assay.

2.9 Trypan blue assay

2×10^5 MCF-7 cells were seeded into each well of a 12-well plate. After 24 h the medium was replaced with 1 mL of fresh medium containing PBS buffer (control) or PCNPs of different concentrations (6.25, 12.5 and 50 μg/mL). The cells were then irradiated with a NIR laser (808 nm, 3 W) after 24 h incubation. The cells was then washed with PBS and stained with trypan blue. Microscopic images of the cells were taken using an Olympus IX73 microscope.

2.10 Cell cycle arrest and apoptosis assay

4×10^5 MCF-7 cells were seeded into each well of 6-well plates and incubated with PBS buffer (control), PCNPs (12.5 and 50 μg/mL) after 24 h post seeding. After NIR irradiation the cells were incubated for another 24 h. After treating with trypsin-EDTA, the cells were collected by centrifugation. The cells were then re-suspended in 70% ethanol for 24 h and stained with propidium iodide for the cell

cycle arrest assay analyzed by Beckman Coulter FC500 flow cytometer using CXP analysis software. For apoptosis assay, the cells were stained with FITC-annexin V and propidium iodide and then analyzed by flow cytometer.

3 Results and discussion

3.1 Synthesis of CNPs and PCNPs

We oxidized AC with 5 M HNO_3 via a 24 h refluxing and obtained yellow fluorescent CDs. Then we synthesized CNPs via fast oxidation cutting of AC within 5 min in which a stronger oxidant fuming HNO_3 associated with concentrated H_2SO_4 was utilized to promote the reaction. The reaction time was largely curtailed compared with similar methods.[30, 32, 36] Production yield of CNPs was determined to be 70%. By cutting down the oxidation time, we expected the as-synthesized CNPs could retain the structure of AC and thus maximize the heritance of the light-absorbing quality from AC.

The size and morphology of the as-prepared CNPs were characterized by TEM and AFM (Fig. 1a). The size of CNPs is mainly distributed in the range of 5-10 nm, and their height in the range of 5-8 nm. Compared with CNPs, the size of CDs is much smaller (less than 3 nm) (Fig. 1b) and their height is about 1 nm, similar to the thickness of single graphene oxide (GO) layer.[37] The results reveal that CNPs produced via 5 min oxidation are much larger than CDs produced via 24 h harsh oxidation, and that the CNPs retain more complete structure of AC than CDs.

A recent study showed that fast (30 s) chemical oxidation yields highly crystalized graphene.[38] In order to investigate the crystallinity of CNPs, several characterizations are conducted. The HR-TEM images (Fig. 1) show that CNPs possess higher crystallinity than CDs. In UV-Vis absorption spectrum of CNPs (Fig. 2a), a typical absorption peak at ca. 230 nm is observed, and the strong background absorption below 300 nm is assigned to the π-π^* transition of aromatic sp^2 domains. Compared with CNPs, the absorption of CDs (Fig. 2a) below 300 nm is relatively low, indicating a small quantity of aromatic sp^2 groups. The structural information of the CNPs and

CDs was obtained by FT-IR spectra (Fig. 2b). For CNPs, carboxyl groups (1730 cm^{-1}), aromatic groups (1603 and 1256 cm^{-1}) and C-O groups (1382 cm^{-1}) are observed. In case of CDs, aromatic groups (1611 cm^{-1}) and C-O groups (1384 cm^{-1}) are clearly seen. XPS analysis indicated that for CDs (Fig. S1a), the percentage of C=C, C-O and C=O are 17.1%, 68.6% and 14.3%, respectively. While for CNPs (Fig. S1b), the percentage of C=C, C=O and C-C are 54%, 26.5% and 19.5%, respectively. The high percentage (68.6%) of C-O in CDs is in agreement with the strong absorption of C-O groups in FT-IR spectra. For CNPs, the high percentage (54%) of C=C indicates the presence of large number of aromatic groups. In the Raman spectra of CDs and CNPs (Fig. S2), the G-band shifts from 1614 cm^{-1} (CDs) to 1606 cm^{-1} (CNPs) due to the increase of layer thickness from CDs to CNPs, which is consistent with the AFM results.

PEG was conjugated to CNPs to form PCNPs. The appearance of IR peaks for PCNPs (Fig. S3a) at around 1730, 1460, 1350 and 1288 cm^{-1} indicates the existence of amide groups, a solid evidence for successful PEG passivation. The peaks at around 2900 and 1105 cm^{-1} correspond to the stretching vibrations of C-H and C-O-C of the PEG moiety, respectively. Calculation based on thermogravimetric (TG) analysis (Fig. S3b) reveals that each CNP was coupled with 3-8 PEG molecules.

The hydrodynamic sizes of CNPs and PCNPs were measured to be 10 and 32 nm, respectively, as shown in Tab. 1. The former is consistent with the size of CNPs determined by TEM and AFM. A substantial increase in hydrodynamic size of PCNPs is due to conjugation of PEG to CNPs. The abundant negative charged carboxyl groups are proved with the negative zeta potential value of CNPs (-54 mV), which transfers to -36 mV after PEG passivation.

The as-synthesized PCNPs were highly soluble in DI water, saline, cell medium (Fig. S4a), and some polar organic solutions (dimethylformamide (DMF), dimethyl sulfoxide (DMSO) and Acetonitrile) as well (Fig. S4b), attributed to the ample oxygen-containing functional groups, such as carboxyl and hydroxyl groups and PEG of PCNPs.

Then we studied the photoluminescence (PL) property of PCNPs and CDs. As can

be seen in Fig. 3, the PL of PCNPs is notably weaker than that of CDs. CDs exhibit strong PL, while PCNPs is nearly a non-emitter, indicating that PCNPs are similar to AC in structure.

Due to the PL property of CDs we speculated that PCNPs had a stronger heat-producing ability than CDs. Upon irradiation using an 808-nm laser, the 200-μL PCNPs solutions at a series of concentrations (6.25, 12.5, 25 and 50 μg/mL) experienced a temperature increase within 5 min (Fig. 4a). Compared with control (PBS, irradiation) whose final temperature is less than 40 ^{o}C, for PCNPs at a concentration of 6.25 μg/mL, the temperature increases 12 ^{o}C after irradiation. At a higher concentration of PCNPs, the temperature rises even more significantly. For PCNPs with concentrations of 12.5, 25 and 50 μg/mL, the temperatures increase by 23, 35 and 41 ^{o}C, respectively. The result indicates that the temperature increases of the PCNPS aqueous solutions are primarily caused by the photothermal effect of PCNPs and concentration-dependent. However, compared with PCNPs, the temperature rise of CDs is much lower than that of PCNPs according to our experiment. The temperatures for CDs solutions are about half of that for PCNPs (Fig. 4b). As we predicted, the PL performance of CDs may spoil their photothermal effect.[33] This result shows that PCNPs have stronger heat-producing ability than CDs, and therefore should have better performances in photothermal cancer ablation. Then we investigated the heat-producing ability of two prevailing materials: gold nanorods (GNR) (Fig. S5a) and graphene oxide (GO) (Fig. S5b). The final temperatures of GNR and GO are 34 ^{o}C and 32 ^{o}C, respectively, which are less than that of PCNPs (41 ^{o}C), indicating that PCNPs possess better heat-producing ability than GNR and GO with the same concentrations, which facilitates their application in photothermal therapy. Our work provides a simple and selective approach to synthesize nonfluorescent, efficient heat-generating PCNPs.

3.2 MTT and LDH release

Dedicated to biomedical applications, the cytotoxicity of PCNPs is a prerequisite issue to study. After incubation of MCF-7 cells with PCNPs of the concentrations

from 3.9 to 250 μg/mL for 24 h, MTT assay (Fig. 5a) indicated that the cell viability does not change significantly compared with the PBS control. This result demonstrates that PCNPs is non-cytotoxic even at the concentration up to 250 μg/mL, which is much higher than the safe doses of carbon nanomaterials reported previously.[14, 32] Apart from cell viability, the possible cell membrane damage induced by PCNPs was also investigated by examining the level of released lactate dehydrogenase (LDH) (Fig. 5b), an indicator of cell membrane damage. The result showed that the levels of released LDH from MCF-7 cells exhibited negligible changes compared with that of the positive control, suggesting that PCNPs has no noticeable damage to membrane integrity. Compared with PCNPs, MTT assay (Fig. S6a) indicates that CNPs are nontoxic to MCF-7 cells, while LDH release assay (Fig. S6b) shows that CNPs exhibit a higher level of LDH release than that of PCNPs, likely due to the lack of PEG which allows CNPs to easily interact with LDH and improve its activity.

3.3 Cellular uptake of PCNPs

Before the photothermal experiment, we investigated the cellular uptake of PCNPs. Due to the non-emitting property of PCNPs, FITC, a bright green fluorescent probe, was anchored on PCNPs to probe intracellular location of PCNPs. The PCNPs-FITC conjugates were synthesized successfully, as evidenced by the UV-Vis (Fig. S7a) and FT-IR spectra (Fig. S3a) of PCNPs-FITC and FITC. The as-synthesized PCNPs-FITC shows strong PL (Fig. S7b), which is feasible for cell imaging. As the result (Fig. 6) indicates, the intracellular fluorescence increases with the incubation time. Compared with control (0 h), few PCNPs-FITC enter cells reporting relatively low intensity fluorescence after 6 h incubation. After 24 h incubation, large accumulation of PCNPs-FITC occurs in the cells, leading to a dramatic increase of fluorescence. The PCNPs are mainly distributed in cytoplasm and difficult to escape from the cells,[39] facilitating long-time photothermal ablation of tumors.

3.4 *In vitro* PTT of PCNPs

Next, we investigated the photothermal effect of PCNPs for *in vitro* cancer cell ablation under NIR laser irradiation. As showed in Fig. 7a, without PCNPs, NIR light exposure causes negligible toxicity to cells compared with the control (PBS, dark). Increased cytotoxicity is observed as the concentration of PCNPs increases. Temperature rises relatively slowly at low concentration of PCNPs (6.25 μg/mL) (Fig. 4a), which causes ca. 30% of cell death. Under increasing temperature (no more than 50 ^{o}C), the cells likely undergo a series of mild damage, including enzyme inactivation and mitochondrial injury, which takes 30-60 min to induce cell death.[40] The number of cells killed can be increased 100-fold with 2 ^{o}C increase.[41] The temperature increases rapidly to more than 60 ^{o}C at relatively high concentrations of PCNPs (25 and 50 μg/mL). Such high temperature can decimate cells within a short time. In this case the cells may undergo some fatal changes including protein denaturation, membrane rupture and cell shrinkage.[5] The laser power density in our study is estimated to be 9 W/cm^2 which is less than the threshold of gold nanorods (10 W/cm^2)[8] which are widely used in PTT and much lower than that for gold nanorods/SiO_2 core/shell composites (24 W/cm^2)[42], revealing the highly efficient photothermal conversion ability of PCNPs. Trypan blue staining was performed to visualize the PTT efficacy of PCNPs, in which the dead cells were shown as blue dots, while live cells were not (Fig. 7b). The proportion of dead cells ascends along with the rise of concentrations of PCNPs, compared with the control (PBS, irradiation). This result is consistent with that of *in vitro* PTT above, revealing the great potential of PCNPs in cancer therapy.

3.5 Cell cycle arrest and apoptosis of MCF-7 cells

To throw light on the mechanism of the ablation of MCF-7 cells by PTT with PCNPs, the cells were stained with propidium iodide in the cell cycle arrest assay (Fig. 8a). After incubation with PCNPs, PTT shows no significant effects on cell cycle of MCF-7 cells. Compared with PBS, few sub-G1 events are observed at 12.5 μg/mL of PCNPs, while significant sub-G1 events occur at higher concentration (50 μg/mL), which indicates the presence of apoptotic cells. The level of cell apoptosis was

examined by Annexin V–propidium iodide staining (Fig. 8b). Upon irradiation, PBS and PCNPs (12.5 μg/mL) have a relatively weak effect on the apoptosis of MCF-7 cells, while incubation with PCNPs at a higher concentration (50 μg/mL) imposes much notable influence on the cell apoptosis. The percentages of apoptotic cells were measured to be ca. 9%, 15% and 60%, respectively, indicating a strong dose-dependent effect on the apoptosis of MCF-7 cells. This result is consistent with the levels of sub-G1 events in cell cycle arrest assay.

4 Conclusion

In summary, we for the first time synthesized water-soluble PCNPs with high production yield and successfully applied them for *in vitro* photothermal ablation of cancer cells. We have shown that the as-synthesized PCNPs are nontoxic to MCF-7 cells and have no side effects on membrane integrity. Then we demonstrated that PCNPs can efficiently convert NIR light into heat to burn cancer cells to death, compared to CDs. Cell cycle arrest and apoptosis assays revealed no notable changes in cell cycle, and a dose-dependent apoptosis. Our results exhibit high potential of PCNPs in efficient PTT of cancer ablation. Further efforts are needed to explore their in vivo PTT efficacy and long-term toxicity toward practical applications.

Acknowledgements

We greatly acknowledge financial support from National Natural Science Foundation of China (No. 51361130033), Ministry of Science and Technology of China (No. 2014CB965000) and the Natural Science Foundation of Jiangsu Province (BK20130350).

Reference

1. H. D. Suit and M. Shwayder, *Cancer*, 1974, **34**, 122-129.
2. J. van der Zee, D. G. Gonzalez, G. C. van Rhoon, J. D. P. van Dijk, W. L. J. van Putten and A. A. M. Hart, *Lancet*, 2000, **355**, 1119-1125.
3. P. Wust, B. Hildebrandt, G. Sreenivasa, B. Rau, J. Gellermann, H. Riess, R.

Felix and P. M. Schlag, *Lancet Oncol.*, 2002, **3**, 487-497.
4. A. M. Smith, M. C. Mancini and S. M. Nie, *Nat. Nanotechnol.*, 2009, **4**, 710-711.
5. M. Nikfarjam, V. Muralidharan and C. Christophi, *J. Surg. Res.*, 2005, **127**, 208-223.
6. D. P. O'Neal, L. R. Hirsch, N. J. Halas, J. D. Payne and J. L. West, *Cancer Lett.*, 2004, **209**, 171-176.
7. G.-S. Park, H. Kwon, D. W. Kwak, S. Y. Park, M. Kim, J.-H. Lee, H. Han, S. Heo, X. S. Li and J. H. Lee, *Nano Lett.*, 2012, **12**, 1638-1642.
8. X. Huang, I. H. El-Sayed, W. Qian and M. A. El-Sayed, *J. Am. Chem. Soc.*, 2006, **128**, 2115-2120.
9. M. S. Yavuz, Y. Cheng, J. Chen, C. M. Cobley, Q. Zhang, M. Rycenga, J. Xie, C. Kim, K. H. Song and A. G. Schwartz, *Nat. Mater.*, 2009, **8**, 935-939.
10. H. Liu, D. Chen, L. Li, T. Liu, L. Tan, X. Wu and F. Tang, *Angew. Chem.*, 2011, **123**, 921-925.
11. X. Wu, T. Ming, X. Wang, P. Wang, J. Wang and J. Chen, *ACS Nano*, 2009, **4**, 113-120.
12. A. Burke, X. Ding, R. Singh, R. A. Kraft, N. Levi-Polyachenko, M. N. Rylander, C. Szot, C. Buchanan, J. Whitney and J. Fisher, *Proc. Natl. Acad. Sci.*, 2009, **106**, 12897-12902.
13. K. Yang, S. Zhang, G. Zhang, X. Sun, S.-T. Lee and Z. Liu, *Nano Lett.*, 2010, **10**, 3318-3323.
14. J. T. Robinson, S. M. Tabakman, Y. Liang, H. Wang, H. Sanchez Casalongue, D. Vinh and H. Dai, *J. Am. Chem. Soc.*, 2011, **133**, 6825-6831.
15. Q. Tian, F. Jiang, R. Zou, Q. Liu, Z. Chen, M. Zhu, S. Yang, J. Wang, J. Wang and J. Hu, *ACS Nano*, 2011, **5**, 9761-9771.
16. C. M. Hessel, V. P. Pattani, M. Rasch, M. G. Panthani, B. Koo, J. W. Tunnell and B. A. Korgel, *Nano Lett.*, 2011, **11**, 2560-2566.
17. H. Yang, H. Mao, Z. Wan, A. Zhu, M. Guo, Y. Li, X. Li, J. Wan, X. Yang, X. Shuai and H. Chen, *Biomaterials*, 2013, **34**, 9124-9133.
18. J. F. Lovell, C. S. Jin, E. Huynh, H. Jin, C. Kim, J. L. Rubinstein, W. C. Chan, W. Cao, L. V. Wang and G. Zheng, *Nat. Mater.*, 2011, **10**, 324-332.
19. L. Cheng, K. Yang, Q. Chen and Z. Liu, *ACS Nano*, 2012, **6**, 5605-5613.
20. Z. Chen, Q. Wang, H. Wang, L. Zhang, G. Song, L. Song, J. Hu, H. Wang, J. Liu and M. Zhu, *Adv. Mater.*, 2013, **25**, 2095-2100.
21. S. P. Sherlock, S. M. Tabakman, L. Xie and H. Dai, *ACS Nano*, 2011, **5**, 1505-1512.
22. A. O. Alaspää, M. J. Kuisma, K. Hoppu and P. J. Neuvonen, *Ann. Emerg. Med.*, 2005, **45**, 207-212.
23. O. E. Orisakwe, N. A. Ilondu, O. J. Afonne, S. I. Ofoefule and C. N. Orish, *Pharmacol. Res.*, 2000, **42**, 167-170.
24. H. A. Spiller and T. S. Sawyer, *J. Emerg. Med.*, 2007, **33**, 141-144.
25. P. Neuvonen, P. Kuusisto, H. Vapaatalo and V. Manninen, *Eur. J. Clin. Pharmacol.*, 1989, **37**, 225-230.

26. S. Watarai and M. Koiwa, *J. Dairy Sci.*, 2008, **91**, 1458-1463.
27. A. Hagiwara, T. Takahashi, K. Kitamura, C. Sakakura, M. Shirasu, M. Ohgaki, T. Imanishi and J. Yamasaki, *J. Gastroenterol.*, 1997, **32**, 141-147.
28. A. E. Giuliano, D. M. Kirgan, J. M. Guenther and D. L. Morton, *Ann. Surg.*, 1994, **220**, 391-401.
29. M. Chu, J. Peng, J. Zhao, S. Liang, Y. Shao and Q. Wu, *Biomaterials*, 2012, **34**, 1820-1832.
30. Y.-P. Sun, B. Zhou, Y. Lin, W. Wang, K. S. Fernando, P. Pathak, M. J. Meziani, B. A. Harruff, X. Wang and H. Wang, *J. Am. Chem. Soc.*, 2006, **128**, 7756-7757.
31. S. K. Bhunia, A. Saha, A. R. Maity, S. C. Ray and N. R. Jana, *Sci Rep*, 2013, **3**, 1-7.
32. J. Peng, W. Gao, B. K. Gupta, Z. Liu, R. Romero-Aburto, L. Ge, L. Song, L. B. Alemany, X. Zhan and G. Gao, *Nano Lett.*, 2012, **12**, 844-849.
33. S. Berciaud, L. Cognet and B. Lounis, *Nano Lett.*, 2005, **5**, 2160-2163.
34. G. L. Kenausis, J. Vörös, D. L. Elbert, N. Huang, R. Hofer, L. Ruiz-Taylor, M. Textor, J. A. Hubbell and N. D. Spencer, *J. Phys. Chem. B*, 2000, **104**, 3298-3309.
35. M. Malmsten, K. Emoto and J. M. Van Alstine, *J. Colloid Interface Sci.*, 1998, **202**, 507-517.
36. H. Liu, T. Ye and C. Mao, *Angewandte Chemie International Edition*, 2007, **46**, 6473-6475.
37. S. Stankovich, D. A. Dikin, G. H. Dommett, K. M. Kohlhaas, E. J. Zimney, E. A. Stach, R. D. Piner, S. T. Nguyen and R. S. Ruoff, *Nature*, 2006, **442**, 282-286.
38. P. L. Chiu, D. D. Mastrogiovanni, D. Wei, C. Louis, M. Jeong, G. Yu, P. Saad, C. R. Flach, R. Mendelsohn and E. Garfunkel, *J. Am. Chem.Soc.*, 2012, **134**, 5850-5856.
39. J. A. Kim, C. Åberg, A. Salvati and K. A. Dawson, *Nat. Nanotechnol.*, 2011, **7**, 62-68.
40. D. Wheatley, C. Kerr and D. Gregory, *Int. J.Hyperthermia*, 1989, **5**, 145-162.
41. R. Cavaliere, E. C. Ciocatto, B. C. Giovanella, C. Heidelberger, R. O. Johnson, M. Margottini, B. Mondovi, G. Moricca and A. Rossi‐Fanelli, *Cancer*, 1967, **20**, 1351-1381.
42. Z. Zhang, J. Wang and C. Chen, *Adv. Mater.*, 2013, **24**, 1418-1423.

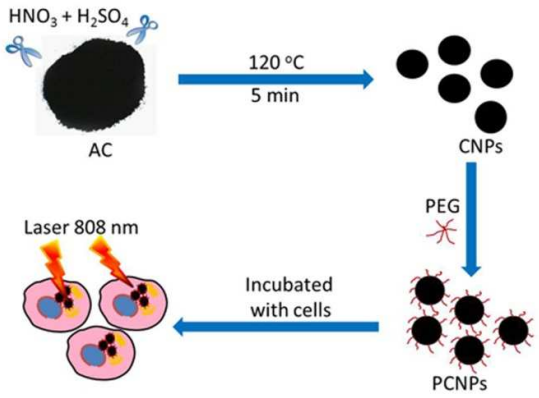

Scheme1. Schematic diagram of preparation of PCNPs and in vitro photothermal therapy.

Figure captions

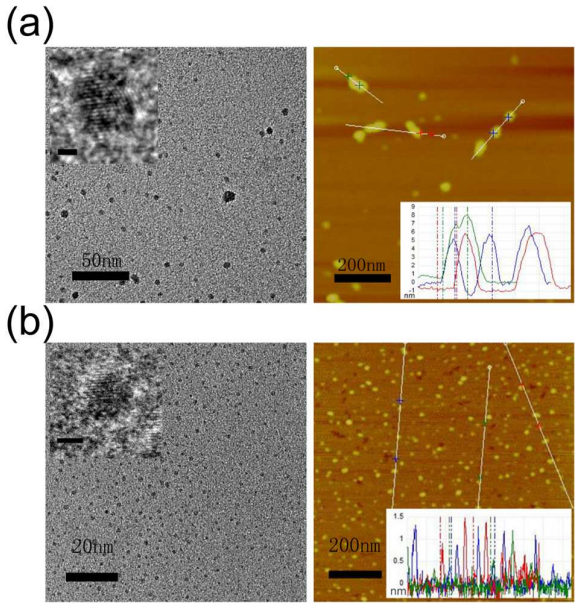

Fig. 1 TEM (left) and AFM (right) images of (a) CNPs and (b) CDs samples, respectively. The insets in TEM images of (a) and (b) are the HR-TEM images of CNPs and CDs samples (scale bar 2 nm), respectively, and the insets in AFM images are height diagrams of CNPs and CDs, respectively.

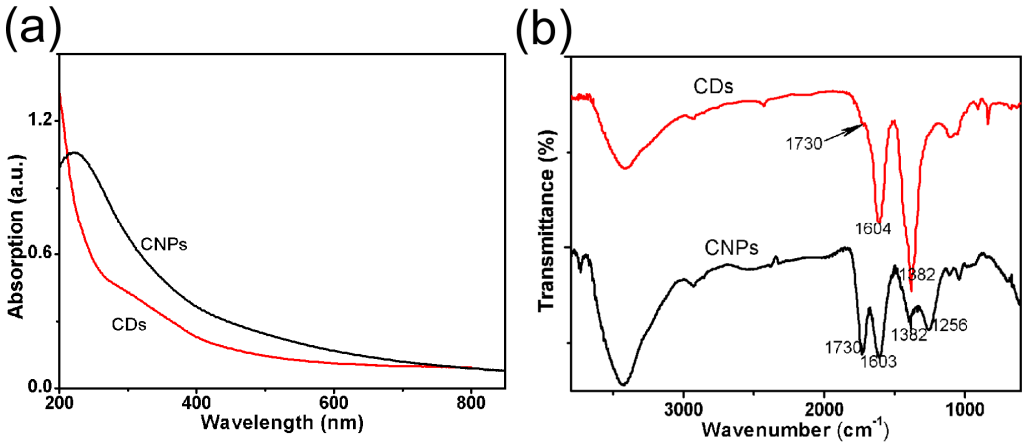

Fig. 2 (a) UV-Vis spectra of CNPs and CDs in aqueous solution. (b) FT-IR spectra of CNPs and CDs.

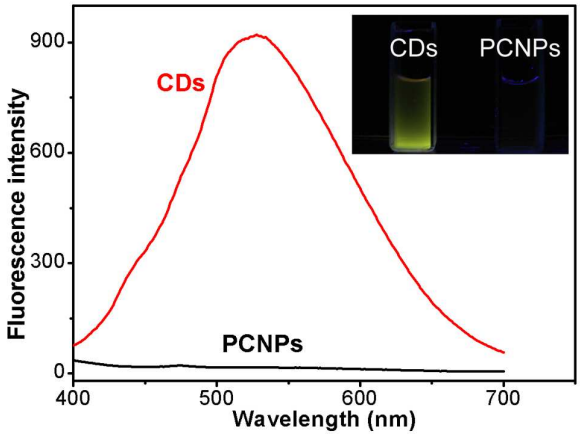

Fig. 3 Photoluminescence spectra of PCNPs and CDs aqueous solutions excited at 365 nm. The inset image is the photograph of the samples in aqueous solution under a 365-nm UV light.

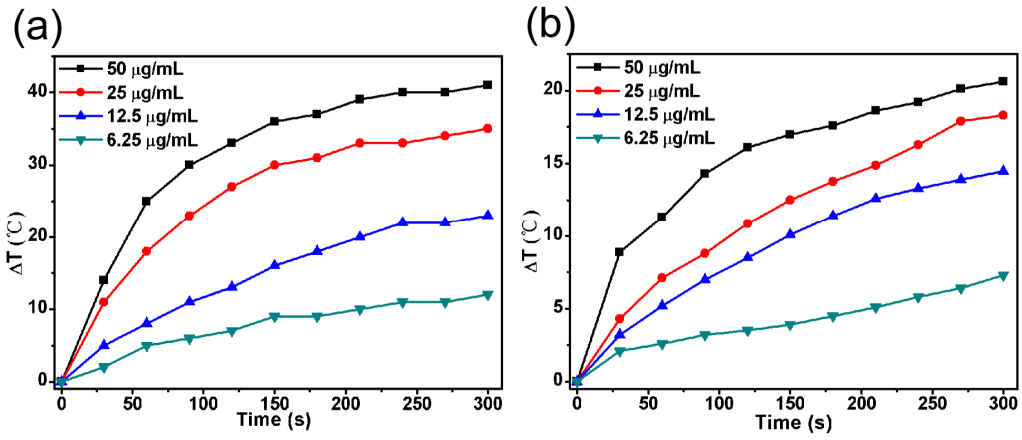

Fig. 4 Photothermal effect of (a) PCNPs and (b) CDs of different concentrations (6.25, 12.5, 25 and 50 μg/mL) under NIR irradiation (808 nm, 3 W) for 5 min. ΔT refers to the temperature difference of PCNPs (or CDs) and DI water under equal irradiation.

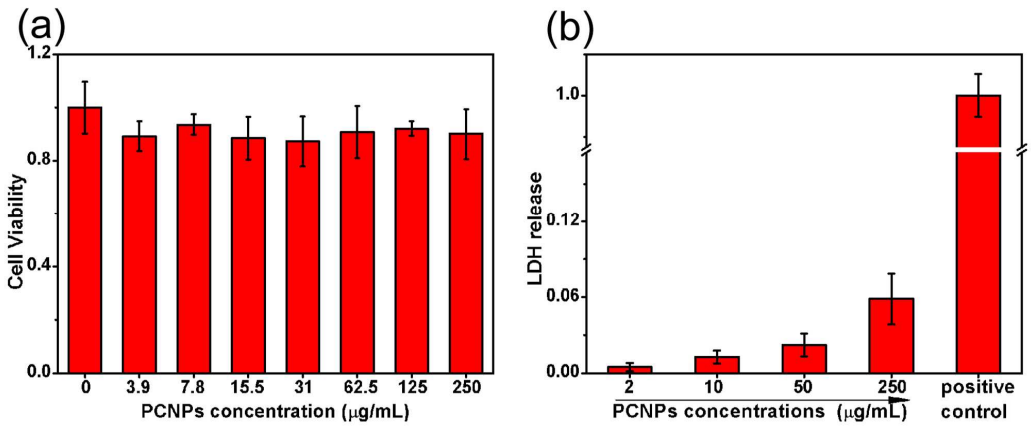

Fig. 5 (a) MTT assay of MCF-7 cells viability treated with PBS or PCNPs of different concentrations (3.9, 7.8, 15.5, 31, 62.5, 125 and 250 μg/mL) for 24 h. (b) LDH release assay of MCF-7 cells treated with PBS or PCNPs of different concentrations (2, 10, 50 and 250 μg/mL) for 24 h. Positive control refers to the maximum LDH release after cell lysis.

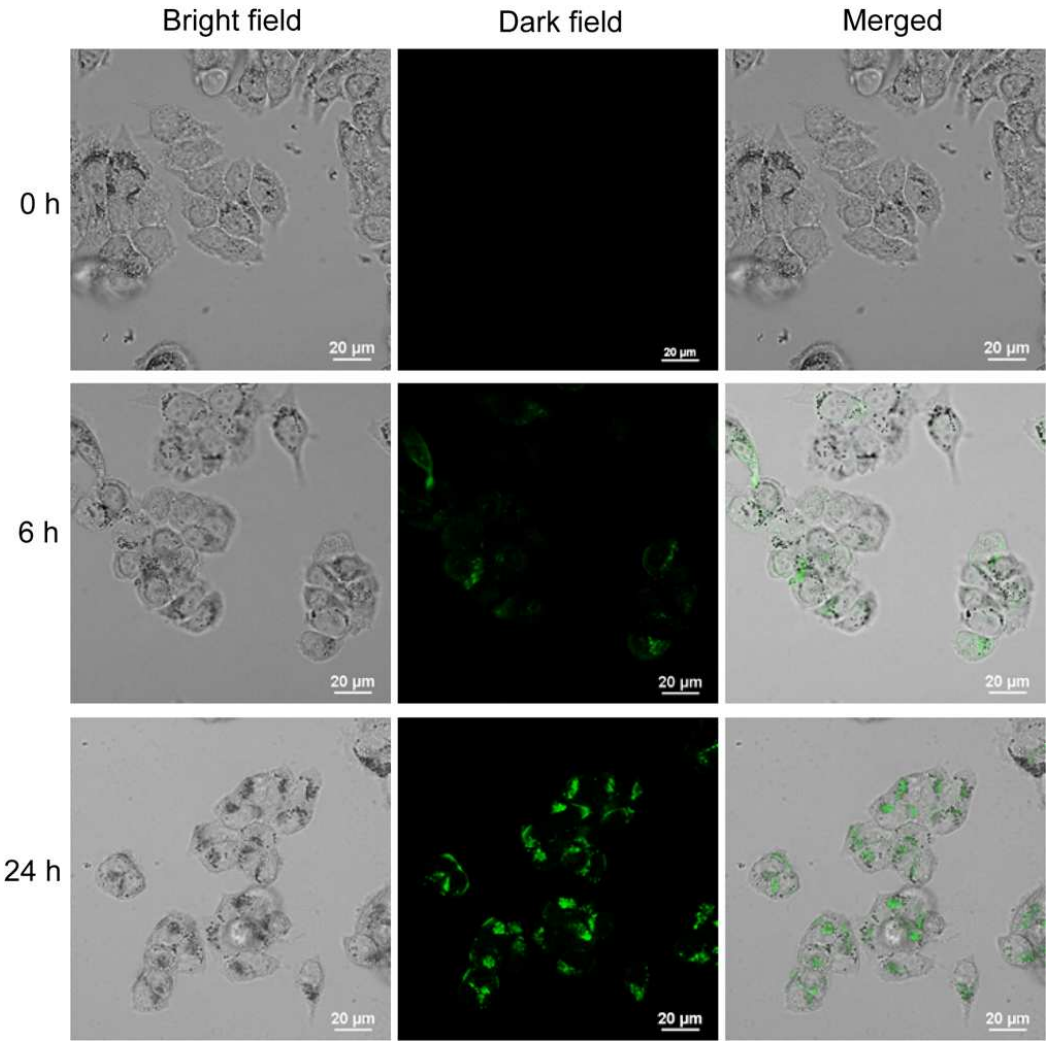

Fig. 6 Confocal microscopic images of MCF-7 cells treated with PBS and PCNPs-FITC for 6 h and 24 h, respectively.

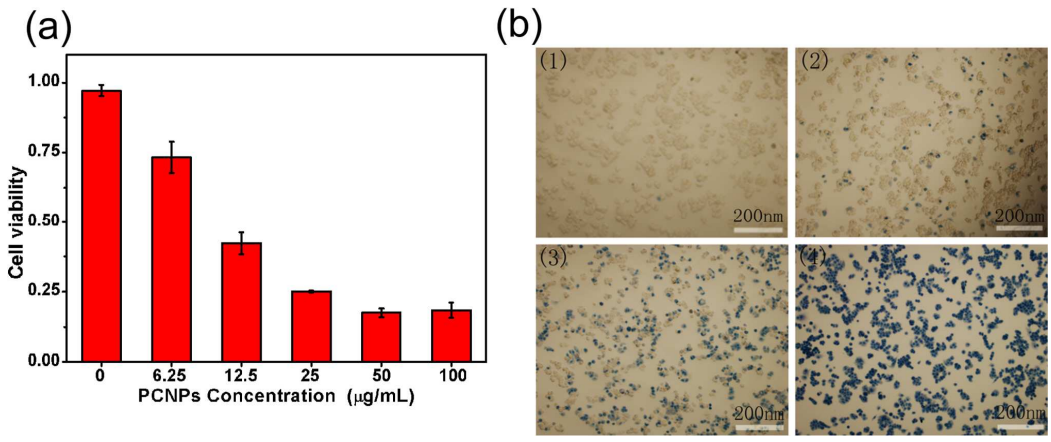

Fig. 7 *In vitro* PTT data using PCNPs. (a) MTT assay of MCF-7 cells viability treated with PBS and PCNPs of different concentrations (6.25, 12.5, 25, 50 and 100 μg/mL) under NIR irradiation (808 nm, 3 W) for 5 min. (b) Trypan blue staining of MCF-7 cells treated with PBS and PCNPs of different concentrations (6.25, 12.5 and 50 μg/mL) under NIR irradiation (808 nm, 3 W). (1) - (4) correspond to PBS and PCNPs with concentrations of 6.25, 12.5 and 50 μg/mL, respectively.

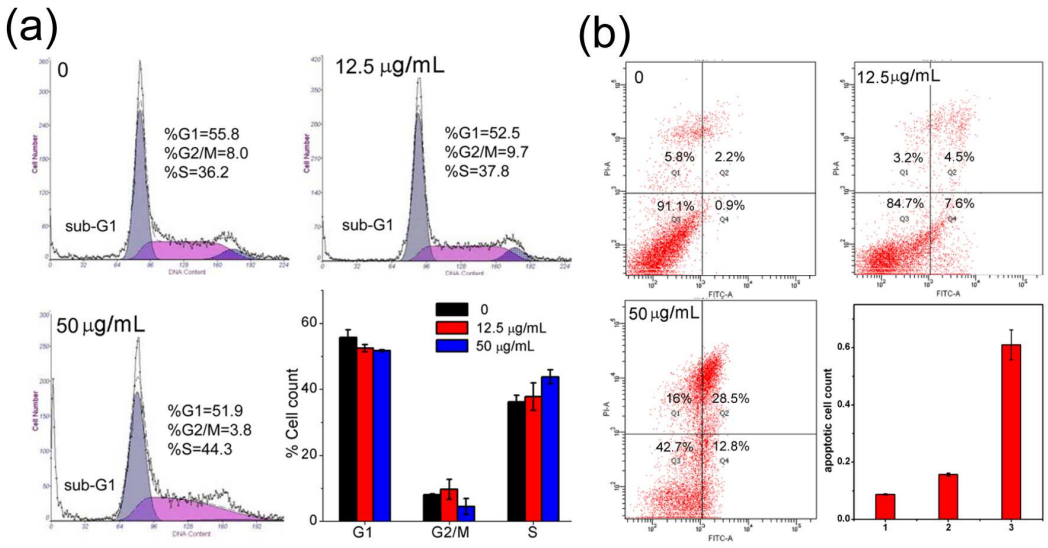

Fig. 8 (a) Cell cycle analysis of MCF-7 cells treated with PBS and PCNPs with concentrations of 12.5 and 50 μg/mL, respectively. (b) The apoptosis of MCF-7 cells induced by PBS and PCNPs with concentrations of 12.5 and 50 μg/mL and the plot of apoptosis levels in which 1-3 refer to PBS and PCNPs with concentrations of 12.5 and 50 μg/mL, respectively.

Tab. 1 Hydrodynamic size and zeta potential of CNPs and PCNPs.

	Hydrodynamic size /nm	Zeta potential /mV
CNPs	10	-54
PCNPs	32	-36